



# A LADH-like Zn-MOF as an efficient bifunctional catalyst for cyanosilylation of aldehydes and photocatalytic oxidative carbon–carbon coupling reaction

Feng Li<sup>1</sup>, Ren Ma<sup>1</sup>, Zhengqiang Xia, Qing Wei<sup>\*\*</sup>, Qi Yang, Sanping Chen<sup>\*</sup>, Shengli Gao

Key Laboratory of Synthetic and Natural Functional Molecule Chemistry of Ministry of Education, Ministry of Education, College of Chemistry and Materials Science, Northwest University, Xi'an, 710127, China



## ARTICLE INFO

### Keywords:

Metal-organic framework  
Cyanosilylation  
Photocatalysis  
Carbon–carbon coupling

## ABSTRACT

The rational design of component and coordination configuration of active center is critical and useful to the development of multifunctional MOF-based catalysts. Herein, a bifunctional Zn-MOF, **Zn-ADBA**, constructed by photoactive 4,4'-(9,10-anthracenediyi)dibenzoic acid ( $H_2\text{ADBA}$ ) ligand and Zn(II) ions, is employed as heterogeneous catalyst for efficient cyanosilylation and photocatalytic oxidative carbon–carbon coupling reactions. The unsaturated Zn(II) centers with strong Lewis acid character can effectively activate aldehyde substrates, which promotes **Zn-ADBA** to catalyze cyanosilylation of electron-withdrawing substituted benzaldehyde with a turnover frequency value up to  $53.1 \text{ h}^{-1}$ . Meanwhile, the photo-functional ADBA<sup>2-</sup> ligands featuring large steric hindrance drive the Zn(II) center adopt the liver alcohol dehydrogenase (LADH) like characteristics, which renders **Zn-ADBA** ( $\lambda_{\text{max}}$  absorption = 406 nm) high-efficient photocatalytic oxidation of N-aryl-tetrahydroisoquinoline substrates with yields above 95% over 4 h under visible light. The recyclability of **Zn-ADBA** and the possible catalytic mechanisms are also systematically investigated by a series of experiments including PXRD, IR, EPR and DFT analyses.

## 1. Introduction

The formation of C–C bonds is one kind of the most fundamental reactions in organic chemistry [1–3], and especially many important pharmaceutical intermediates and fine chemicals have been prepared by the transition metal-catalyzed carbon–carbon coupling reactions, due to the special coordination addition mechanisms and high selectivity [4–6]. However, some direct C–C bond formations are still challenging tasks even under extreme conditions owing to the typically unreactive C–H bonds [7–9]. Photocatalytic organic synthesis, a green synthesis approach, can provide powerful molecular activation modes and highly active free radicals to promote the above-mentioned impossible bond constructions under mild conditions [10–12]. For example, Luo et al. realized the asymmetric cross-dehydrogenative coupling of tertiary amines and ketones under the action of visible light [13]. In view of the different advantages of the two catalytic activation pathways, it is highly promising to develop bifunctional catalysts that integrate photocatalysis and metal catalysis to realize convenient and efficient C–C bond formations.

Metal–organic frameworks, a class of porous hybrid materials with infinite network structures built from organic bridging ligands and inorganic metal nodes, are attractive candidates as bifunctional catalysts because of the large specific surface areas, flexible structures, and abundant active sites [14–22]. The diversity of components makes it possible to incorporate both photocatalytic unit and catalytic metal unit into a same framework [23,24]. On one hand, the metal nodes with unsaturated coordination environment can be used as strong Lewis acid sites to easily initiate the coordination addition activation [25–27]. On the other hand, the optical functional ligands can absorb photons to transfer photogenerated electrons, and the resulting photoactive species further reduce/oxidize substrates into active radicals [28,29]. In addition, the intrinsic porosity of MOF produces an advantage confined micro-environment to effectively fix and stabilize the active radicals and increase the reaction selectivity [30]. Therefore, the integration of photoactive organic ligands and coordination unsaturated metals within a single MOF is an effective strategy to achieve the bifunctional catalyst for photocatalysis and metal catalysis.

The rigid conjugate organic molecules tend to initiate photogenerated

\* Corresponding author.

\*\* Corresponding author.

E-mail addresses: [weiqq@126.com](mailto:weiqq@126.com) (Q. Wei), [sanpingchen@126.com](mailto:sanpingchen@126.com) (S. Chen).

<sup>1</sup> These authors contributed equally to this work.

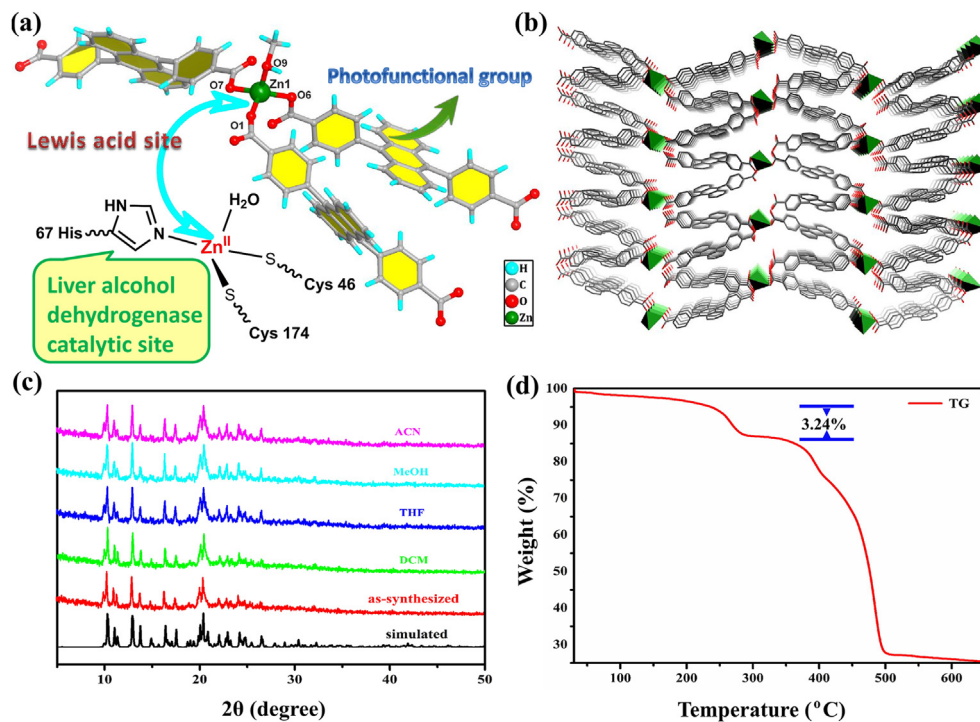


**Fig. 1.** (a) Tetracoordinated Zn(II) center in Zn-ADBA featuring potential LADH-like and Lewis acid catalytic activity. (b) 3D supramolecular structure of Zn-ADBA. (c) PXRD patterns of the as-synthesized Zn-ADBA and the samples after being dispersed in different solvents. (d) TG curve of Zn-ADBA.

electrons upon illumination and exhibit good photoactivity, because their intrinsic carbon atoms connected by  $sp^2$  hybrid orbitals can effectively reduce the energy level difference between bonding and anti-bonding electron orbitals [31]. Herein, a largely conjugated ligand, 4, 4'-(9,10-anthracenediyi)dibenzoic acid ( $H_2$ ADBA), with an absorption band in visible light was synthesized to construct a bifunctional Zn-MOF, Zn-ADBA, under solvothermal conditions, which was used for efficiently catalyzing the cyanosilylation of aromatic aldehydes and the C-C coupling reaction of N-aryl-tetrahydroisoquinoline and nitromethane. Zn-ADBA exhibits a 3D supramolecular architecture with 1D infinite chains, in which the distorted tetrahedron coordination configuration of Zn(II) center featuring strong Lewis acidity displays a high catalytic yield range of 92.3–95.6% for the cyanosilylation of aromatic aldehydes with electron-withdrawing groups. Meanwhile, the twisted configuration of  $H_2$ ADBA drives zinc center to adopt a coordination geometry analogous to that of the active Zn(II) center in liver alcohol dehydrogenase (LADH) [32], which renders Zn-ADBA photoactivity for the efficient photooxidation of N-aryl-tetrahydroisoquinoline with a yield as high as 98.8% under mild reaction conditions. Moreover, the durability of the catalyst was also checked.

## 2. Experimental

### 2.1. Materials and methods

All chemicals and reagents were obtained from commercial sources and were used without further purification.  $H_2$ ADBA and the N-aryl-tetrahydroisoquinoline substrates were synthesized according to the literature methods.[33, 34]  $^1$ H NMR spectra was recorded using a 400 MHz nuclear magnetic resonance spectrometer (Bruker AV500). Elemental analyses (C, H, and N) were performed on an Elemental Vario EL III analyzer. Fourier transform infrared (FT-IR) spectra were recorded from KBr pellets using a Bruker Vertex 70 FI-IR spectrometer in the range of 4000–400  $\text{cm}^{-1}$ . Thermogravimetric analysis (TGA) was performed on a Q600 SDT thermal analyzer with a heating rate of 10  $^{\circ}\text{C min}^{-1}$  from 30 to 800  $^{\circ}\text{C}$  under a flow of nitrogen. Powder X-ray diffraction (PXRD) data

was obtained on a Bruker D8 ADVANCE X-ray powder diffractometer ( $\text{Cu K}\alpha$  radiation,  $\lambda = 1.5418 \text{ \AA}$ ) at 60 KV and 300 mA. The photocurrent test was performed on a CHI660E electrochemical workstation under UV-vis light irradiation with 20 s light on-off cycles. The working electrode prepared from Zn-ADBA and 5% Nafion was immersed in 0.02 M  $\text{Na}_2\text{SO}_4$  aqueous solution. UV-visible absorption spectra were recorded on a Lambda 750s UV-vis spectrophotometer. Electron paramagnetic resonance (EPR) spectra were recorded at room temperature using a Bruker ESP-300E spectrometer at 9.8 GHz, X-band, with 100 Hz field modulation. All calculations were carried out by the Gaussian 09 software package [35]. In the calculations, The HOMO, LUMO and HOMO-LUMO gaps are calculated by DFT calculations ( $wB97XD^2/6-31G^*$ ). Metal atoms use the effective nuclear LanL2DZ basis set, and other atoms use the 6-31G\* basis set. The dimensional plots of molecular configurations and orbitals were generated with the GaussView program [36].

### 2.2. Synthesis of Zn-ADBA

A mixture of  $H_2$ ADBA (20.9 mg, 0.05 mmol) and  $\text{Zn}(\text{Ac})_2 \cdot 2\text{H}_2\text{O}$  (11.0 mg, 0.05 mmol) was dissolved in 6 mL of mixed solvent of DMF/ $\text{H}_2\text{O}/\text{CH}_3\text{OH}$  (1:1:1, v/v/v). The mixture was sealed in a 10 mL Teflon-lined stainless-steel autoclave and heated at 120  $^{\circ}\text{C}$  for 48 h. After cooling to room temperature at a rate of 5  $^{\circ}\text{C h}^{-1}$ , yellow block crystals were collected, washed with DMF and  $\text{H}_2\text{O}$ , and dried in air. Yield: 52.8% (based on  $H_2$ ADBA). Elemental analysis (EA) calcd. for Zn-ADBA ( $C_{61}H_{52}N_2O_9Zn$ ,  $M_r = 1022.42$ ): C 71.65%, H 5.12%, N 2.73%; Found: C 71.21%, H, 4.99%, N 2.58%. IR (KBr,  $\text{cm}^{-1}$ ): 3424(m), 3064(m), 2438(w), 1600(vs), 1523(vs), 1379(vs), 1172(m), 1016(m), 837(m), 749(m), 660(m).

### 2.3. X-ray Crystallography

Single-crystal X-ray data of Zn-ADBA were collected on a Bruker smart APEXII CCD diffractometer, equipped with graphite-monochromatized  $\text{Mo K}\alpha$  radiation ( $\lambda = 0.71073 \text{ \AA}$ ) by using  $\omega$  and  $\varphi$  scan mode. The data were processed using the Siemens SAINT program

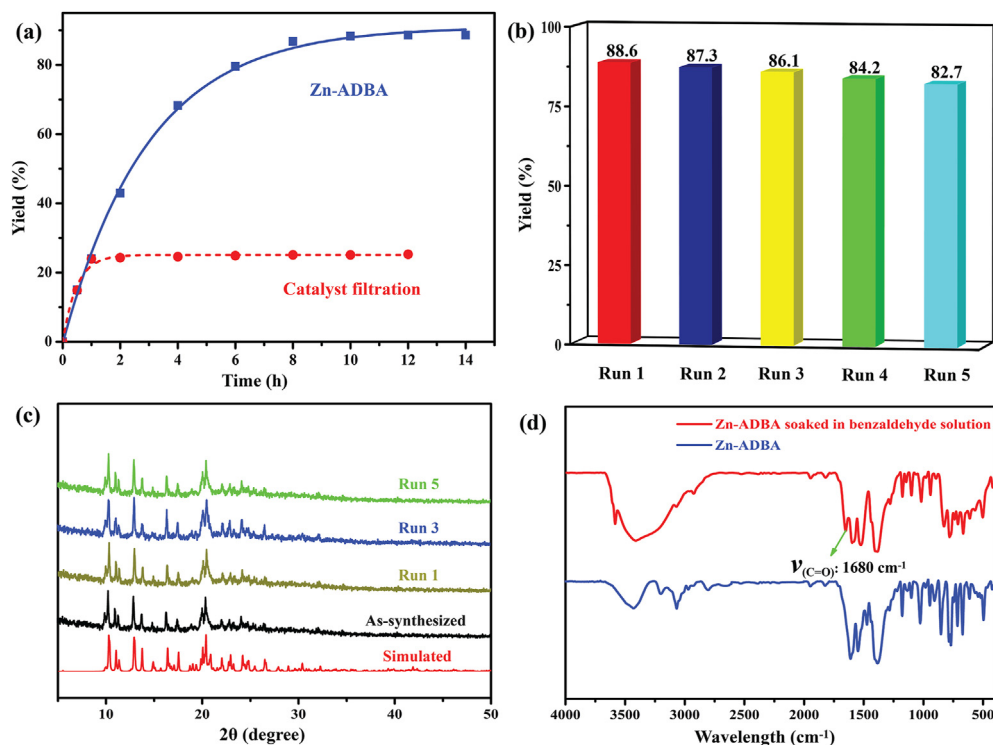


**Fig. 2.** (a) Catalytic traces of the cyanosilylation of benzaldehyde performed by Zn-ADBA filtered after 12 h under the optimal conditions. (b) Recycling catalytic experiments of the cyanosilylation of benzaldehyde catalyzed by Zn-ADBA under the optimum conditions. (c) PXRD patterns of the recycled Zn-ADBA after five runs of the cyanosilylation reaction. (d) IR spectra of Zn-ADBA before and after absorbing benzaldehyde.

and absorption corrections were carried out using the SADABS program [37]. The structure was solved by direct methods with SHELXS and refined on  $F^2$  by full-matrix least-squares using SHELXL-97 [38]. All of the non-hydrogen atoms were placed from the Fourier maps and refined anisotropically. Hydrogen atoms were placed in geometrically calculated positions and refined as part of a riding model. The detailed structural data and refinement parameters are summarized in Table S1.

#### 2.4. Typical procedure for the cyanosilylation of aromatic aldehydes

Zn-ADBA ( $6 \times 10^{-3}$  mmol) was placed into a 50 mL round-bottom flask with dry dichloromethane (10.0 mL) followed by the addition of aldehyde (2 mmol). After stirring for 10 min at 25 °C, trimethylsilylcyanide (2.4 mmol) was added into the suspension and the resulting mixture was stirred for the next 12 h. Upon completion of the reaction, the catalyst was removed by filtration, washed with dichloromethane three times, and then collected by centrifugation for catalyzing a new batch. The organic filtrate was directly evaporated, and the residue was purified by column chromatography on silica gel using petroleum ether/ethyl acetate (1:5, v/v) as the eluent to give the pure product.

#### 2.5. Typical procedure for the reaction of N-aryl-tetrahydroisoquinoline with nitromethane

A mixture of N-aryl-tetrahydroisoquinoline (0.2 mmol), Zn-ADBA (10.2 mg, 0.01 mmol) and  $\text{CH}_3\text{NO}_2$  solvent (3.0 mL) was added to a 10 mL quartz glass tube equipped with a magnetic stir bar in an oxygen atmosphere. The reaction was stirred and placed ~10 cm away from a 30 W fluorescent lamp for 4 h of irradiation. After completion of the reaction, the catalyst was separated by centrifugation, washed with methanol and dichloromethane, dried in a vacuum for further reuse. The solvent was removed under vacuum and the reaction mixture was diluted with water and extracted with dichloromethane. The combined organic phases were washed with  $\text{Na}_2\text{S}_2\text{O}_3$  (aq), dried with anhydrous  $\text{Na}_2\text{SO}_4$ ,

concentrated in vacuo, and purified by column chromatography on silica gel with n-hexane/ethyl acetate (10:1, v/v) as the eluent to obtain the yellow product.

### 3. Results and discussion

#### 3.1. Structure and stability characterization

Single crystal X-ray diffraction analysis shows that Zn-ADBA crystallizes in the monoclinic crystal system with  $P2_1$  space group. The asymmetric unit of Zn-ADBA consists of a crystallographically independent Zn(II) ion, two fully deprotonated  $\text{ADBA}^{2-}$  ligands, two free dimethylamine cations and a coordinated methanol molecule. As shown in Fig. 1a, each Zn(II) ion is four coordinated by four oxygen atoms from three ligands and a methanol molecule to form a disordered tetrahedral coordination geometry configuration (Fig. 1a), wherein the exposed unsaturated sites can be used as potential Lewis acid catalytic active centers. The Zn(II) centers are further connected by  $\text{ADBA}^{2-}$  ligands with a  $\mu_2\text{-}\eta^1\text{-}\eta^1$  carboxylate bridging mode to yield one-dimensional chains (Fig. S1). The shortest intrachain Zn-Zn<sup>\*</sup> separation is 17.89(3) Å. Eventually, these chains stack each other to generate a three-dimensional supramolecular architecture (Fig. 1b). It should be noted that the  $\text{ADBA}^{2-}$  ligands feature highly torsional fashions with large dihedral angles of 71.11(8)° and 84.98(5)° between anthracene plane and benzene ring (Fig. S2), and the resulting large steric hindrance drives the Zn(II) center to adopt the similar structural characteristics with the liver alcohol dehydrogenase (LADH) (Fig. 1a) [39]. Such LADH-mimicked Zn(II) sites render Zn-ADBA potential photooxidation activity for high-efficient photocatalytic application.

As depicted in Fig. 1c, the power X-ray diffraction (PXRD) patterns of the as-synthesized Zn-ADBA agree well with the simulated ones, indicating the high phase purity of the bulk samples. As shown in Fig. 1d, Zn-ADBA experiences a weight loss of 3.24% from 250 °C to 283 °C, which could be ascribed to the loss of the solvent molecules (calcd. 3.13%). The

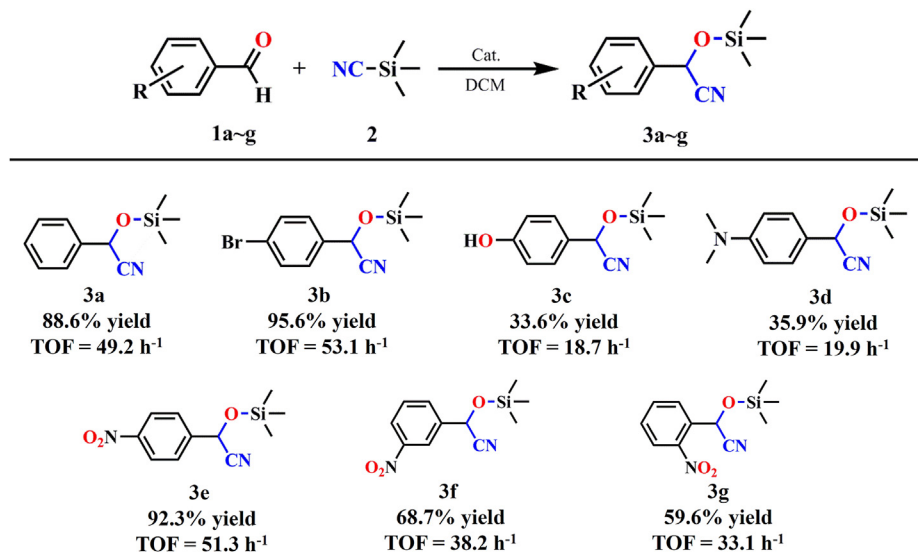


Fig. 3. Cyanosilylation of aromatic aldehydes with Zn-ADBA as catalyst. The yields were determined by  $^1\text{H}$  NMR analysis.

remaining substances keep stable up to 388 °C, probably due to the strong electrostatic interactions between the dimethylamine cations and the Zn-ADBA anion framework [40]. Additionally, the samples were immersed in several different solvents, including MeOH, DCM, THF and ACN, for two days, to verify the solvent stability of Zn-ADBA. All the PXRD patterns of the samples with solvent dispersed are consistent with the simulated patterns, indicating that the skeletons of Zn-ADBA can be well maintained in multiple solvents. The good thermal and chemical stability endow Zn-ADBA with great potential as heterogeneous catalyst for chemical transformations.

### 3.2. Cyanosilylation of aldehydes

The cyanosilylation reaction of benzaldehyde and trimethylsilyl cyanide (TMSCN) (molar ratio = 1:1.2) was used as a model reaction to

check the potential Lewis acid catalytical activity of the coordinated unsaturated Zn(II) sites of Zn-ADBA. The optimization of the reaction conditions was carried out with Zn-ADBA as the catalyst. When the amount of catalyst increases from 3 to 5 mol%, the yield does not increase significantly, so the optimal amount of catalyst is 3 mol% (entries 4–6 in Table S2 and Fig. S3). As shown in Table S2 and Fig. S4, the DCM system exhibits the highest catalytic yield. Additionally, when the temperature increases from 25 to 35 °C and the reaction time increases from 12 to 14 h, no significant yield increase occurs (Fig. S5). Therefore, a 0.3 mol% loading of catalyst used in dichloromethane at 25 °C for 12 h was determined to be the best option. As shown in Fig. 2a,  $^1\text{H}$  NMR analysis revealed that Zn-ADBA acting as an effective catalyst afforded an 88.6% yield under the optimal reaction conditions, and the catalytic efficiency is superior to those of many MOF-based catalytic systems (Table S3). The removal of Zn-ADBA by filtration after 2 h shut down the reaction, and

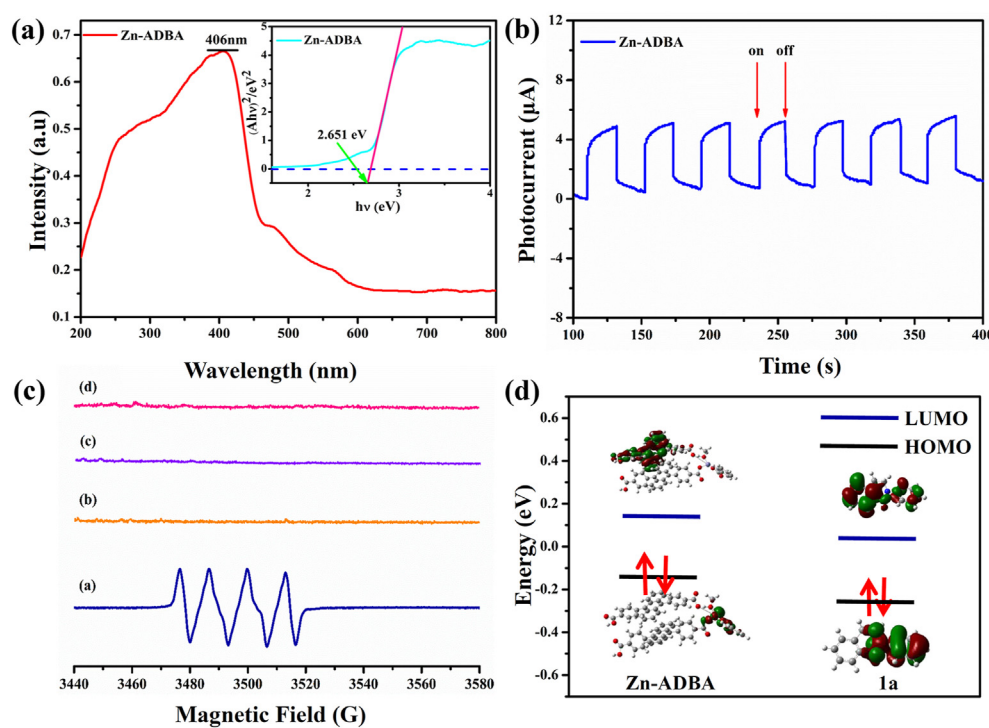


Fig. 4. (a) Solid-state UV-vis absorption and Kubelka-Munk-transformed reflectance (inset) spectra of Zn-ADBA. (b) Transient photocurrent response of Zn-ADBA under visible-light irradiation. (c) EPR measurements of Zn-ADBA in  $\text{CH}_3\text{NO}_2$  with (blue line) and without (orange line) N-phenyl-tetrahydroisoquinoline in the presence of DMPO upon irradiation for 30 s in air atmosphere; EPR measurements of Zn-ADBA in  $\text{CH}_3\text{NO}_2$  without (purple line) and with (fuchsia line) N-phenyl-tetrahydroisoquinoline in the presence of TEMP upon irradiation for 30 s in air atmosphere. (d) Molecular orbital energy diagrams and isodensity surface plots of the frontier orbitals of Zn-ADBA. (For interpretation of the references to colour in this figure legend, the reader is referred to the Web version of this article.)

**Table 1**

Optimization of the reaction conditions and control catalytic experiments for the **Zn-ADBA** catalyzed CDC reaction.<sup>a</sup>

Entry	Catalyst	Cat (mol %)	Yield (%)
1	<b>Zn-ADBA</b>	1	47.9
2	<b>Zn-ADBA</b>	3	79.8
3	<b>Zn-ADBA</b>	5	97.6
4	<b>Zn-ADBA</b>	7	98.1
5	<b>Zn-ADBA</b> (in dark)	5	trace
6	None	-	4.3
7	H <sub>2</sub> ADBA	5	17.8
8	Zn(Ac) <sub>2</sub> ·2H <sub>2</sub> O	5	19.3
9	Zn(Ac) <sub>2</sub> ·2H <sub>2</sub> O + H <sub>2</sub> ADBA	5	26.6

<sup>1</sup>H NMR analysis.

<sup>a</sup> The yields were determined by.

there was no further conversion in the filtrate for another 10 h at the same conditions (Fig. 2a). The result indicated that there were no active species leaching into the catalytic system and **Zn-ADBA** was a true heterogeneous catalyst. In addition, the recyclability of the MOF catalyst was demonstrated by five cycles of experiments. Upon completion of the reaction, the catalyst could be easily isolated from the reaction suspension by simple centrifugation and washing, and directly reused in a new round of reaction. As depicted in Fig. 2b, **Zn-ADBA** solids can be reused at least five times without a significant loss of reactivity (88.6–82.7% yield). The PXRD patterns of the reused catalyst matched well with the simulated patterns from the single crystal X-ray diffraction data of **Zn-ADBA**, showing that the framework and crystallinity of **Zn-ADBA** were well maintained after the catalytic reaction (Fig. 2c). Control experiments revealed that a very low background reaction (<5% yield) was observed in the absence of catalyst, and the only use of same equiv. of ligand H<sub>2</sub>ADBA or Zn(Ac)<sub>2</sub>·2H<sub>2</sub>O led to a yield of 18.8% or 20.9%, respectively. Even when a mixture of metal and ligand (1:2) was added, only a small increase to 26.6% yield was obtained (entries 16–18, Table S2). These results suggested that the special coordination between ADBA<sup>2-</sup> and Zn(II) played a critical role in the catalytic reaction, which greatly activated the aldehyde group of substrates as Lewis acid catalytic site. Such carbonyl activation was further confirmed by the IR spectrum of **Zn-ADBA** immersed in a DCM solution containing benzaldehyde (Fig. 2d). The shift of the characteristic C=O stretching vibration peak from 1690 cm<sup>-1</sup> (free benzaldehyde) to 1680 cm<sup>-1</sup> indicated that the catalyst has an effective activation effect on the substrate benzaldehyde [41].

When para-substituted aromatic aldehydes were used as substrates (1a–1e), a broad yield range of 33.6–95.6% was achieved in the **Zn-ADBA** reaction systems, suggesting a significant electron effect on the reaction yield. The aryl aldehydes with electron withdrawing nitro- and brom-species at the para position gave high reaction yields of 92.3% and 95.6%, respectively, while those with electron donating dimethylamino- and hydroxyl-groups at the para position respectively exhibited very low yields of 33.6% and 35.9% (Fig. 3). The result may be because that the electron cloud is closer to the electron-withdrawing species to expose the lone pair of electrons of carbonyl oxygen when electron-withdrawing groups substituted benzaldehydes used, leading to high activity of the aldehyde group [42–44]. Additionally, for the nitro-substituted benzaldehydes, the effects of steric hindrance are also investigated (1e–1g). The reaction yield decreased with the increase of the steric hindrance, and the o-nitrobenzaldehyde system gave a lowest yield of 59.6%.

### 3.3. Photocatalytic C–C coupling reaction of N-aryl-tetrahydroisoquinoline with nitromethane

Before testing the photooxidation activity of **Zn-ADBA**, the photo-response capacity of **Zn-ADBA** was investigated by UV-Vis diffuse reflectance spectroscopy and photocurrent analyses. As shown in Fig. 4a,

**Zn-ADBA** shows broad absorption bands range from the ultraviolet to visible light regions with a maximum absorption peak of 406 nm in the solid state, which maybe correspond to the n–π\* and π–π\* transition of H<sub>2</sub>ADBA ligands [45]. Based on the Kubelka-Munk function [46], the optical band gap of **Zn-ADBA** was determined to be 2.651 eV (Fig. 4a inset), exhibiting great photocatalytic potential. Fig. 4b shows the transient photocurrent intensities of **Zn-ADBA** with several repeating cycles of intermittent on-off irradiation. It is clear that the **Zn-ADBA** catalyst displays a powerful transient photocurrent response to visible light, which could be attributed to the effective generation, separation, and migration of photoinduced charge carriers in **Zn-ADBA** [47]. Therefore, the visible-light driven aerobic cross dehydrogenative coupling (CDC) reaction of N-phenyl-tetrahydroisoquinoline and nitromethane was selected as a model reaction to check the photocatalytic performances of **Zn-ADBA**. As shown in Table 1, upon irradiation (30 W fluorescent lamp) at 25 °C in the presence of air as oxygen source over 4 h, the reaction yields quickly increased with the amount of catalyst increasing from 1 to 5 mol%, and no obvious yield increase was found when the amount further increases to 7 mol% (Fig. S7). It was also found that the yield of the extended reaction did not increase significantly after 4 h, suggesting that a 5 mol% loading of catalyst and a reaction time of 4 h are the optimal reaction conditions, and the reaction system giving a high yield of 97.6% (Fig. S8). The catalyst was filtered out after 2 h of reaction, the filtrate afforded only 8% additional yield for another 2 h at the same reaction conditions, confirming the typical inhomogeneity of the photocatalytic reaction.

Control experiment revealed that almost no product was observed when the reaction was carried out in the dark, and only a 4.3% of yield was detected when there was no catalyst, which demonstrated that both the photocatalyst and the light are indispensable for the efficient progress of the coupling reaction. When the same equivalent of metal or ligand is used, the yields are 17.8% and 19.3%, respectively, and the yield of the mixture system of metal and ligand (1:2) is only 26.6% (Table 1). In addition, the stability of **Zn-ADBA** for photocatalytic conversion can be confirmed by recycling experiments (Fig. S9). The solid of **Zn-ADBA** separated from the reaction suspension by simple filtration can be reused at least five times with insignificant loss of activity (84.3% of yield after five cycles). The PXRD patterns of **Zn-ADBA** isolated from the reaction mixture further confirmed the well-retained skeleton (Fig. S10). It has been reported that both the superoxide radical anion (O<sub>2</sub><sup>•-</sup>) and singlet oxygen (<sup>1</sup>O<sub>2</sub>) may be the key active species in the coupling reaction. As a result, the electron paramagnetic resonance (EPR) tests were performed to confirm the active oxygen species in the photocatalytic reaction by employing 5,5-dimethyl-1-pyrrolidine-N-oxide (DMPO) and 2,2,6,6-tetramethyl-1-piperidine (TEMP) as catching agents. As shown in Fig. 4c, no signal was observed upon irradiation of the mixture containing TEMP and **Zn-ADBA** in the absence or presence of N-phenyl-tetrahydroisoquinoline, indicating that no <sup>1</sup>O<sub>2</sub> was generated in the reaction process. There was also no signal when DMPO was added to a CH<sub>3</sub>NO<sub>2</sub> solution of **Zn-ADBA**, whereas the signal of O<sub>2</sub><sup>•-</sup> captured by using DMPO as a radical scavenger was clearly detected in the presence of N-phenyl-tetrahydroisoquinoline. The results demonstrate that O<sub>2</sub><sup>•-</sup> is the active species during the catalytic process.

Based on the experimental results and previous reports [48,49], a possible reaction mechanism is proposed (Fig. S11): upon illumination, **Zn-ADBA** changes to its excited state through the electronic transition, and the electrons in the excited state lack electrons to capture the electrons on the N atom in N-aryl-tetrahydroisoquinoline to form ammoniated cationic groups. The electron-derived **Zn-ADBA** reacts with oxygen to obtain a superoxide anion radical (O<sub>2</sub><sup>•-</sup>), and O<sub>2</sub> oxidizes the sp<sup>3</sup> C–H bond of the nitrogen atom in the adjacent amine to obtain an imine ion intermediate. On this basis, the imine ion is captured by a nucleophile to obtain the corresponding C–C coupling product. Herein, the probability of electron transfer between **Zn-ADBA** and N-phenyl-tetrahydroisoquinoline was calculated by density functional theory (DFT) to verify the reaction possibility. DFT calculations (Fig. 4d) show

**Table 2**Photocatalytic C–C coupling reactions of N-aryl-tetrahydroisoquinolines and nitromethane.<sup>a</sup>

Entry	Substrate	Product	Yield (%)
1			97.6
2			96.8
3			98.8
4			98.4
5			97.9
6			97.5

<sup>a</sup> <sup>1</sup>H NMR analysis.<sup>a</sup> The yields were determined by.

that the lowest unoccupied molecular orbital (LUMO) of **Zn-ADBA** fragment (0.1344 eV) lies in higher energy than the LUMO of N-phenyl-tetrahydroisoquinoline (0.0487 eV), and the highest occupied molecular orbital (HOMO) of **Zn-ADBA** fragment (~0.1297 eV) lies in lower energy than the HOMO of N-phenyl-tetrahydroisoquinoline (~0.2753 eV), indicating that the efficient electron transfer may occur from N-phenyl-tetrahydroisoquinoline to **Zn-ADBA**. To further illustrate the above-mentioned mechanism, a variety of N-aryl-tetrahydroisoquinolines were subjected to the optimized reaction conditions; and all the desired coupling products were obtained in more than 90% yields (Table 2). Obviously, the introduction of both electron-donating and -accepting groups on the phenyl ring has little effect on the reaction yields.

#### 4. Conclusions

In summary, a new 3D supramolecular Zn-MOF catalyst (**Zn-ADBA**) was solvothermally synthesized and structurally characterized. The photo-functional ADBA<sup>2-</sup> ligands react with Zn(II) ions to generate the special tetracoordinated LADH-like configuration with strong Lewis acid and photocatalytic oxidation activity, which renders **Zn-ADBA** acting as bifunctional heterogeneous catalyst for effectively catalyzing the cyanosilylation of different aromatic aldehydes and the carbon-carbon coupling reactions between N-aryl-tetrahydroisoquinolines and nitromethane with good recyclability. This present work provides an enlighten thought for the design and development of highly efficient bifunctional MOF-based catalysts for acid-base catalytic and photocatalytic conversions. In our laboratory, further research is underway to expand the range of organic conversions using **Zn-ADBA** as a catalyst.

#### Supporting information

Crystal structure and data as well as the PXRD patterns of **Zn-ADBA**, catalytic results and mechanisms, <sup>1</sup>H NMR data of substrates and catalytic products are available. CCDC-2082631 (**Zn-ADBA**) contains the supplementary crystallographic data for this paper. These data can be obtained free of charge from the Cambridge Crystallographic Data Center via [www.ccdc.cam.ac.uk/data\\_request/cif](http://www.ccdc.cam.ac.uk/data_request/cif) (or from the Cambridge Crystallographic Data Center, 12 Union Road, Cambridge CB2 1EZ, UK; fax: +(44) 1223-336-033; e-mail: [deposit@ccdc.cam.ac.uk](mailto:deposit@ccdc.cam.ac.uk)).

#### Author contributions

The manuscript was written through contributions of all authors. All authors have given approval to the final version of the manuscript.

#### CRediT authorship contribution statement

**Feng Li:** Investigation, Writing – original draft, preparation. **Ren Ma:** Validation, Writing – original draft, preparation. **Zhengqiang Xia:** Conceptualization, Writing – original draft, preparation. **Qing Wei:** Conceptualization, Writing-Reviewing and Editing. **Qi Yang:** Formal analysis. **Sanping Chen:** Conceptualization, Writing-Reviewing and Editing, Supervision, Resources. **Shengli Gao:** Supervision.

#### Declaration of competing interest

No conflict of interest exists in the submission of this manuscript, and the manuscript is approved by all authors for publication. All the authors

listed have approved the enclosed manuscript and declared that the work described is an original research that has not been published previously, and not under consideration for publication elsewhere, in whole or in part.

## Acknowledgements

This work was financially supported by the National Natural Science Foundation of China (Nos. 21727805 and 21803042), the Nature Science Basic Research Program of Shaanxi (Nos. 2019JQ-067 and 2019JM-079), the 64th China Postdoctoral Science Foundation Funded Project (2018M643706), and the Shaanxi Province Postdoctoral Research Project.

## Appendix A. Supplementary data

Supplementary data to this article can be found online at <https://doi.org/10.1016/j.jssc.2021.122337>.

## References

- [1] B. Rao, R. Kinjo, Boron-based catalysts for C–C bond–formation reactions, *Chem. Asian J.* 13 (2018) 1279–1292.
- [2] J. Liu, X.Y. Xiong, J. Chen, Y.T. Wang, R.R. Zhu, J.H. Huang, Double C–H activation for the C–C bond formation reactions, *Curr. Org. Synth.* 7 (2018) 882–903.
- [3] A. Batra, K.N. Singh, Recent developments in transition metal–free cross-dehydrogenative coupling reactions for C–C Bond Formation, *Eur. J. Org. Chem.* 43 (2020) 6676–6703.
- [4] S.H. Shi, Y.J. Liang, J. Ning, Electrochemical oxidation induced selective C–C bond cleavage, *Chem. Rev.* 121 (2021) 485–505.
- [5] J.H. Wang, S.A. Blaszczy, X.X. Li, W.P. Tang, Transition metal-catalyzed selective carbon–carbon bond cleavage of vinylcyclopropanes in cycloaddition reactions, *Chem. Rev.* 121 (2021) 110–139.
- [6] B.M. Trost, J.T. Mastersa, Transition metal-catalyzed couplings of alkynes to 1,3-enynes: modern methods and synthetic applications, *Chem. Soc. Rev.* 45 (2016) 2212–2238.
- [7] C.K. John, T. Rovis, Amide-directed photoredox-catalysed C–C bond formation at unactivated  $\text{sp}^3$  C–H bonds, *Nature* 539 (2016) 272–275.
- [8] J.L. Liu, X.Y. Xiong, J. Chen, Y.T. Wang, R.R. Zhu, J.H. Huang, Double C–H activation for the C–C bond formation reactions, *Curr. Org. Synth.* 15 (2018) 882–903.
- [9] S. Bag, D. Maiti, Palladium-Catalyzed olefination of aryl C–H bonds by using directing scaffolds, *Synthesis* 48 (2016) 804–815.
- [10] C. Michelin, N. Hoffmann, Photocatalysis applied to organic synthesis—a green chemistry approach, *Curr. Opin. Green. Sust.* 10 (2018) 40–45.
- [11] D. Friedmann, A. Hakki, H. Kim, W.Y. Choi, D. Bahnenmann, Heterogeneous photocatalytic organic synthesis: state-of-the-art and future perspectives, *Green Chem.* 18 (2016) 5391–5411.
- [12] T. Hering, A.U. Meyer, B. König, Photocatalytic anion oxidation and applications in organic synthesis, *J. Org. Chem.* 81 (2016) 6927–6936.
- [13] Q. Yang, L. Zhang, C. Ye, S.Z. Luo, L.Z. Wu, C.H. Tung, Visible-light-promoted asymmetric cross-dehydrogenative coupling of tertiary amines to ketones by synergistic multiple catalysis, *Angew. Chem. Int. Ed.* 13 (2017) 3694–3698.
- [14] C.F. Qiao, L. Lü, W.F. Xu, Z.Q. Xia, C.S. Zhou, S.P. Chen, S.L. Gao, Synthesis, Thermal decomposition kinetics and detonation performance of a three-dimensional solvent-free energetic Ag(I)-MOF, *Acta Phys. Chim. Sin.* 36 (2020) 1905085.
- [15] Q.R. Shen, X.X. Li, R. Li, Y.L. Wu, Application of metal–organic framework materials and derived porous carbon materials in catalytic hydrogenation, *ACS Sustain. Chem. Eng.* 48 (2020) 17608–17621.
- [16] Y.R.S. Joanne, S.S. William, Z.Y. Wang, H.J. Jiang, Metal–organic frameworks: structures and functional applications, *Mater. Today Off.* 27 (2019) 43–68.
- [17] S.A. Razavi, A. Morsali, Linker functionalized metal–organic frameworks, *Coord. Chem. Rev.* 399 (2019) 213023–213080.
- [18] A. Dhakshinamoorthy, Z.H. Li, H. Garcia, Catalysis and photocatalysis by metal organic frameworks, *Chem. Soc. Rev.* 47 (2018) 8134–8172.
- [19] K.B. Wang, Z.K. Wang, J.D. Liu, C. Li, F.F. Mao, H. Wu, Q.C. Zhang, Enhancing the performance of a battery-supercapacitor hybrid energy device through narrowing the capacitance difference between two electrodes via the utilization of 2D MOF-nanosheet-derived Ni@nitrogen-doped-carbon core-shell rings as both negative and positive electrodes, *ACS Appl. Mater. Interfaces* 12 (2020) 47482–47489.
- [20] K.B. Wang, Q. Xun, Q.C. Zhang, Recent progress in metal–organic frameworks as active materials for supercapacitors, *Energy* 2 (2020) 100025.
- [21] K.B. Wang, S.E. Wang, J.D. Liu, Y.X. Guo, F.F. Mao, H. Wu, Q.C. Zhang, Fe-based coordination polymers as battery-type electrodes in semi-solid-state battery-supercapacitor hybrid devices, *ACS Appl. Mater. Interfaces* 13 (2021) 15315–15323.
- [22] K.B. Wang, Q.Q. Li, Z.J. Ren, C. Li, Y. Chu, Z.K. Wang, M.D. Zhang, H. Wu, Q.C. Zhang, 2D Metal–organic frameworks (MOFs) for high-performance BatCap hybrid devices, *Small* 16 (2020) 2001987.
- [23] W.M. Liao, J.H. Zhang, Z. Wang, S.Y. Yin, M. Pan, H.P. Wang, C.Y. Suab, Post-synthetic exchange (PSE) of UiO-67 frameworks with Ru/Rh half-sandwich units for visible-light-driven  $\text{H}_2$  evolution and  $\text{CO}_2$  reduction, *J. Mater. Chem. A* 6 (2018) 11337–11345.
- [24] H.L. Zhu, D.X. Liu, D.T. Zou, J.Y. Zhang, The photo-, electro- and photoelectro-catalytic properties and application prospects of porous coordinate polymers, *J. Mater. Chem. A* 6 (2018) 6130–6154.
- [25] Ü Kökçam-Demir, A. Goldman, L. Esrafil, M. Gharib, A. Morsali, O. Weingart, C. Janiak, Coordinatively unsaturated metal sites (open metal sites) in metal–organic frameworks: design and applications, *Chem. Soc. Rev.* 49 (2020) 2751–2798.
- [26] Y.Y. Li, T.Y. He, R.R. Dai, Y.L. Huang, X.P. Zhou, T.F. Chen, D. Li, Bifunctional gyroidal MOFs: highly efficient Lewis base and Lewis acid catalysts, *Chem. Asian J.* 14 (2019) 3682–3687.
- [27] Z.G. Hu, D. Zhao, Metal–organic frameworks with Lewis acidity: synthesis, characterization, and catalytic applications, *CrystEngComm* 19 (2017) 4066–4081.
- [28] X.L. Chen, Y. Kuwahara, K. Mori, C. Louis, H. Yamashita, A hydrophobic titanium doped zirconium-based metal organic framework for photocatalytic hydrogen peroxide production in a two-phase system, *J. Mater. Chem. A* 4 (2020) 1904–1910.
- [29] X.K. Wang, J. Liu, L. Zhang, L.Z. Dong, S.L. Li, Y.H. Kan, D.S. Li, Y.Q. Lan, Monometallic catalytic models hosted in stable metal–organic frameworks for tunable  $\text{CO}_2$  photoreduction, *ACS Catal.* 9 (2019) 1726–1732.
- [30] W.J. Chen, B.H. Cheng, Q.T. Sun, H. Jiang, Preparation of MOF confined Ag nanoparticles for the highly active, size selective hydrogenation of olefins, *ChemCatChem* 7 (2018) 3659–3665.
- [31] D.J. Li, Z.G. Gu, J. Zhang, Auto-controlled fabrication of a metal-porphyrin framework thin film with tunable optical limiting effects, *Chem. Sci.* 11 (2020) 1935–1942.
- [32] L. Zeng, T. Liu, C. He, D.Y. Shi, F.L. Zhang, C.Y. Duan, Organized aggregation makes insoluble perylene diimide efficient for the reduction of aryl halides via consecutive visible light-induced electron-transfer processes, *J. Am. Chem. Soc.* 138 (2016) 3958–3961.
- [33] P. Sutar, W.M. Suresh, T.K. Maji, Tunable emission in lanthanide coordination polymer gels based on a rationally designed blue emissive gelator, *Chem. Commun.* 51 (2015) 9876–9879.
- [34] M.R. Patil, N.P. Dedhia, A.R. Kapdi, A.V. Kumar, Cobalt(II)/N-hydroxyphthalimide-catalyzed cross-dehydrogenative coupling reaction at room temperature under aerobic condition, *J. Org. Chem.* 83 (2018) 4477–4490.
- [35] M.J. Frisch, G.W. Trucks, H.B. Schlegel, G.E. Scuseria, M.A. Robb, J. Cheeseman, R.G. Scalmani, V. Barone, B. Mennucci, G.A. Petersson, H. Nakatsuji, M. Caricato, X. Li, H.P. Hratchian, A.F. Izmaylov, J. Bloino, G. Zheng, J.L. Sonnenberg, M. Hada, M. Ehara, K. Toyota, R. Fukuda, J. Hasegawa, M. Ishida, T. Nakajima, Y. Honda, O. Kitao, H. Nakai, T. Vreven, J.A. Montgomery, J.E. Peralta, F. Ogliaro, M. Bearpark, J.J. Heyd, E. Brothers, K.N. Kudin, V.N. Staroverov, R. Kobayashi, J. Normand, K. RagHAVACHARI, A. Rendell, J.C. Burant, S.S. Iyengar, J. Tomasi, M. Cossi, N. Rega, J.M. Millam, M. Klene, J.E. Knox, J.B. Cross, V. Bakken, C. Adamo, J. Jaramillo, R. Gomperts, R.E. Stratmann, O. Yazev, A.J. Austin, R. Cammi, C. Pomelli, J.W. Ochterski, R.L. Martin, K. Morokuma, V.G. Zakrzewski, G.A. Voth, P. Salvador, J.J. Dannenberg, S. Dapprich, A.D. Daniels, Ö. Farkas, J.B. Foresman, J.V. Ortiz, J. Cioslowski, D.J. Fox, Gaussian 09, Revision C.01, Gaussian Inc., Wallingford, CT, 2010.
- [36] J. Chai, M. Head-Gordon, Long-range corrected hybrid density functionals with damped atom–atom dispersion corrections, *Phys. Chem. Chem. Phys.* 10 (2008) 6615–6620.
- [37] G.M. Sheldrick, SADABS, Program for Empirical Absorption Correction for Area Detector Data, University of Göttingen, Göttingen, Germany, 1996.
- [38] G.M. Sheldrick, SHELLXS-97, Program for X-Ray Crystal Structure Determination, University of Göttingen, Germany, 1997.
- [39] G. Parkin, Synthetic analogues relevant to the structure and function of zinc enzymes, *Chem. Rev.* 104 (2004) 699–768.
- [40] N. Ren, F. Wang, J.J. Zhang, X.F. Zheng, Progress in thermal analysis kinetics, *Acta Phys. Chim. Sin.* 36 (2020) 1905062.
- [41] Y.X. Wang, H.M. Wang, P. Meng, D.X. Song, J.J. Hou, X.M. Zhang, An uncoordinated tertiary nitrogen based tricarboxylate calcium network with Lewis acid–base dual catalytic sites for cyanosilylation of aldehydes, *Dalton Trans.* 50 (2021) 1740–1746.
- [42] Z.G. Zhang, J.W. Chen, Z.B. Bao, G.G. Chang, H.B. Xing, Q.L. Ren, Insight into the catalytic properties and applications of metal–organic frameworks in the cyanosilylation of aldehydes, *RSC Adv.* 5 (2015) 79355–79360.
- [43] A. Karmakar, G.M.D.M. Rubio, A. Paul, M.F.C. Guedes da Silva, K.T. Mahmudov, F.I. Guseinov, S.A.C. Carabineiro, A.J.L. Pombeiro, Lanthanide metal organic frameworks based on dicarboxyl-functionalized arylhydrazone of barbituric acid: syntheses, structures, luminescence and catalytic cyanosilylation of aldehydes, *Dalton Trans.* 46 (2017) 8649–8657.
- [44] A. Karmakar, S. Hazra, M.F.C. Guedes da Silva, A.J.L. Pombeiro, Synthesis, structure and catalytic application of lead(II) complexes in cyanosilylation reactions, *Dalton Trans.* 44 (2015) 268–281.
- [45] D.B. Shi, Y.W. Ren, H.F. Jiang, J.X. Lu, X.F. Cheng, A new three-dimensional metal–organic framework constructed from 9,10-anthracene dibenzoate and Cd(II) as a highly active heterogeneous catalyst for oxidation of alkylbenzenes, *Dalton Trans.* 42 (2013) 484–492.

- [46] Q. Li, D.X. Xue, Y.F. Zhang, Z.H. Zhang, Z.W. Gao, J.F. Bai, A dual-functional indium–organic framework towards organic pollutant decontamination via physically selective adsorption and chemically photodegradation, *J. Mater. Chem. A*, 5 (2017) 14182–14190.
- [47] Y.F. Zhi, S. Ma, H. Xia, Y.M. Zhang, Z. Shi, Y. Mu, X.M. Liu, Construction of donor–acceptor type conjugated microporous polymers: a fascinating strategy for the development of efficient heterogeneous photocatalysts in organic synthesis, *Appl. Catal., B* 244 (2019) 36–44.
- [48] Q.Y. Li, Z. Ma, W.Q. Zhang, J.L. Xu, W. Wei, H. Lu, X.S. Zhao, X.J. Wang, AIE-active tetraphenylethene functionalized metal–organic framework for selective detection of nitroaromatic explosives and organic photocatalysis, *Chem. Commun.* 52 (2016) 11284–11288.
- [49] H.P. Liang, Q. Chen, B.H. Han, Cationic polycarbazole networks as visible-light heterogeneous photocatalysts for oxidative organic transformations, *ACS Catal.* 8 (2018) 5313–5322.